A CELL CULTURE MODEL OF MRPS2-RELATED CUTIS LAXA

by

Martin Daniel Requena

BA, Cornell University, 2013

Submitted to the Graduate Faculty of

the Department of Human Genetics

Graduate School of Public Health in partial fulfillment

of the requirements for the degree of

Master of Science

University of Pittsburgh

2017

UNIVERSITY OF PITTSBURGH

GRADUATE SCHOOL OF PUBLIC HEALTH

This thesis was presented

by

Martin Requena

It was defended on

April 27, 2017

and approved by

Quasar Saleem Padiath, PhD, MBBS, Assistant Professor, Department of Human Genetics, Graduate School of Public Health, University of Pittsburgh

Eric Goetzman, PhD, Associate Professor, Cell Biology and Molecular Physiology School of Medicine, University of Pittsburgh

Thesis Director: Zsolt Urban, PhD, Associate Professor, Department of Human Genetics, Graduate School of Public Health, University of Pittsburgh

Zsolt Urban, PhD

A CELL CULTURE MODEL OF MRPS2-RELATED CUTIS LAXA

Martin Daniel Requena, MS

University of Pittsburgh, 2017

ABSTRACT

Cutis laxa (CL) is a disorder with multiple etiologies characterized by defective or deficient production of elastin. Previous research has suggested that a significant portion of cases of CL are due to some type of mitochondrial dysfunction. Recent clinical cases implicate mitochondrial ribosomal protein S2 (MRPS2) as a possible cause of autosomal recessive CL. Despite this, in vitro tissue culture knockout of MRPS2 has not been seriously investigated as a model for studying the pathology of mitoribosomal mutation-caused wrinkly skin at a cellular and tissue level. In this study, we used CRISPR/Cas9 to lower the activity of MRPS2 in rat lung fibroblasts. We generated one heterozygous mutant with a mutation in one allele of exon 4, and two biallelic mutants, each with unique mutations in both alleles of exon 3. The biallelic mutations resulted in aberrant mRNA products, including skipping of exon 3 in both biallelic mutants and insertion/deletion mutations unique to each mutant. Analysis of secreted protein and lysate by immunoblotting revealed two MRPS2 fragments, around 8 and 33 kilodaltons in mass, respectively. Immunostaining of biallelic mutant cell lines revealed altered organization and reduced abundance of elastic fibers along with alterations in nuclear and cellular morphology and cell growth rates.

Public Health Significance: The study of the importance of mitoribosomal assembly for fibroblast health has consequences for both the study of cutis laxa and the more general study of the molecular pathogenesis of skin wrinkling.

TABLE OF CONTENTS

LIST OF TABLES

LIST OF FIGURES

PREFACE

Thanks to members of the Padiath Lab, the Gollin Lab, the Adibi Lab, the Roman Lab, and the Urban Lab for their help. Special thanks to Elizabeth Lawrence for generating the Myc-tagged MRPS2 protein and to Dr. Zsolt Urban for his invaluable mentorship.

1.0 BACKGROUND

1.1 THE EXTRACELLULAR MATRIX

The extracellular matrix (ECM) is the superstructure of molecules that connect and support cells in a multicellular organism. Far from being an inert, homogenous scaffold envisioned by early biologists, the ECM is a dynamic and complex system of proteoglycans, polysaccharides, and proteinaceous fibers that support the healthy development of individual cells. The ECM supports the proliferation of fibroblasts by clearing harmful reactive oxygen species, mediating pH, hydration, ionic concentration, and supplying optimal levels of growth factors and other hormones. (Freedman et al., 2015) (Chuang et al., 2014)In addition to providing structural support and a scaffold for cells, networks of extracellular proteins signal cells to grow, divide, enter senescence, or undergo apoptosis by providing signals via transmembrane proteins. A complex network of fibers, mainly elastin and fibrillin, interact at the molecular and fibrillar levels to give the elastic tissues their unique biomechanical properties. (Chuang et al., 2014)In addition to being an important component of skin, elastic fibers play a critical role in the proper function of large arteries and lungs. (Baldwin et al., 2013)

1.2 ELASTIN

Elastin is a polymer with a complex supramolecular structure, and is composed of monomers of the polypeptide tropoelastin. In mammals, there is only one tropoelastin gene, *ELN*, which contains 34 exons. (Rosenbloom et al., 1995)These exons are expressed as various isoforms, and 13 specific isoforms have been identified in the lungs, the skin, the heart, the large arteries, the cartilage and the muscles (http://www.uniprot.org/uniprot/P15502). Due to the large size of the elastin polymers, elastin assembly occurs largely in the extracellular space. As effective exocytosis of large quantities of tropoelastin is necessary for proper elastic fiber biosynthesis, vesicular transport is one stage of the elastin biosynthesis pathway that is often found to be disrupted in wrinkly skin disease (Urban and Davis, 2014).

1.3 FIBRILLIN

In addition to elastin, the fibrillins are the second major component of elastic fibers (Davis and Summers, 2012). Humans have three elastin genes (*FBN1*, *FBN2*, *FBN3*). The *FBN1* gene is the predominant form of fibrillin, a 350 kilodalton glycoprotein(Sakai et al., 1986). Fibrillin monomers assemble into 10-12 nm microfibril, which provide a scaffold for the deposition of tropoelastin (Jensen et al., 2012)In addition to their structural role, the microfibrils contain essential binding domains for growth factors, the disruption of which can result in signaling changes that contribute to diseases such as Marfan syndrome (Bolar et al., 2012).

1.4 CUTIS LAXA

Cutis laxa is a disease with multiple etiologies characterized by deficiency in the production of healthy elastic fibers (Berk et al., 2012). Symptoms can range from simple superficial laxity of skin to fatal cardiovascular and pulmonary dysfunction. The majority of cases of cutis laxa are thought to be hereditary, but in only about 40% of cases is a single gene implicated. Of the cases with a certain genetic cause, roughly 10% of cases involve a mutation in the *ELN* gene itself. Other, less common subtypes reflect the cellular pathways involved in the secretion of elastic fibers and maintenance of the extracellular matrix. Mutations in the ATPase 6 gene, an ATP-powered proton pump responsible for maintaining pH in secretory vesicles, is one significant cause of cutis laxa. Another gene that has been implicated is the ATPase 7, which is responsible for maintaining Cu^{2+} ion transport. Mutations in the latent transforming growth factor beta binding protein 4 (*LTBP4*) gene, have also been identified as a cause in several cases of cutis laxa (Urban and Davis, 2014).

1.5 MITOCHONDRIAL DISEASE

Mitochondrial disorders are genetically and phenotypically heterogeneous, with severity ranging from subclinical deficits in energy to death at the embryonic stage. About 15% of diagnosed cases of mitochondrial disease can be attributed to mutations in the mitochondrial genome itself, which codes for mitochondrial tRNAs, certain core electron transport chain (ETC) proteins, while the rest are caused by mutations in nuclear genes coding for the other ~1500 proteins present in the mitochondrion(Hatakeyama and Goto, 2016). Variation in manifestations

is considerable, even between people with the same mutation, and lesions generally affect tissues and organs with higher energy requirements such as the liver, the muscles, and the nervous system, especially the brain, ears, and eyes. Diagnosed mitochondrial diseases have a prevalence of about 1:5000, but as they are often not recognized by physicians, the actual number could be higher (Liang et al., 2014).

1.6 MITOCHONDRIAL RIBOSOMES

Human mitochondrial ribosomes are distinct from their cytoplasmic counterparts in many ways. Human mitochondrial ribosomes are less massive than human cytoplasmic ribosomes; they are about the same molecular mass as prokaryotic ribosomes but most of the mass in human mitochondrial ribosomes is protein subunits compared to prokaryotic ribosomes where a greater proportion of the ribosome is composed of rRNA(De Silva et al., 2015). A significant portion of the extra protein serves the function of replacing rRNA, which makes up a smaller proportion of the mitoribosome when compared to both the mammalian cytoplasmic ribosome and the *E. coli* ribosome (Koc et al., 2001).The mitochondrial ribosomal protein genes are located in the nucleus, and the proteins contain a localization signal that is cleaved upon import into the mitochondrion (Luciano and Geli, 1996) (Oshima et al., 2005). In the ophistokonts (a phylogenetic group which includes metazoans and fungi) the mitoribosome is permanently tethered to the mitochondrial membrane, while in plants it floats freely in the intermembrane space. The mitochondrial ribosomes are responsible for translating mRNAs that code for 13 proteins in the electron transport chain The mitochondrial genome also contains genes for 22 tRNAs and 2 ribosomal RNAs (Shokolenko and Alexeyev, 2015). Because the electron transport

chain is responsible for oxidative phosphorylation of ATP, defects in mitochondrial ribosome proteins can impair production of electron transport chain proteins, leading to defective OXPHOS. The effects of defects in mitochondrial protein synthesis can range from embryonic lethality to slightly lowered energy, and can affect every organ system (Shokolenko and Alexeyev, 2015). Though most mitochondrial diseases involve many organ systems, many MRPs have tissue-specific isoforms that are mediated by alternative proteolysis, defects in which can lead to disorders of a single tissue or organ system. (Nouws et al., 2016)(Williams et al., 2014)

1.7 MITOCHONDRIAL RIBOSOMAL PROTEIN S2

MRPS2's possible relevance to wrinkly skin disorders became apparent when two unrelated families with cutis laxa were found to have biallelic mutations in the gene (Wevers et al., personal communication). Subjects in these two families presented with hypoglycemia, sensorineural hearing impairments, and mild developmental delay. Taken together, these symptoms suggest some mitochondrial involvement, and exome sequencing of these two individuals revealed that both patients had mutations in the gene MRPS2. Previously, mutations in MRPS16 and MRPS22 had been linked to wrinkly skin, but not MRPS2. In both cases, the patients' parents were unrelated and the disease appears to have been inherited in an autosomal recessive fashion. One patient is a compound heterozygote with a mutation at c.328C>T (p.Arg110Cys) and a mutation at c.340G>A(p.Asp114Asn) and the other patient is homozygous for sequence variant c.413G>A (p.Arg138His)

Not very much is known about MRPS2, specifically, as the bulk of studies on the mitoribosomes have focused on the proteins in aggregate. RNAseq studies have found a number of associations between various diseases and up- or down- regulation of various mitochondrial ribosomal subunit proteins. MRPS2 has been found to be upregulated in bladder and colorectal cancers, and downregulated in head and neck cancers (Gopisetty and Thangarajan, 2016). Based on sequence information, the MRPS2 gene contains 5 exons, though the coding region only starts late in exon 2. The MRPS2 gene does not appear to be very heavily conserved compared to cytosolic ribosomal protein subunit genes. The homology between murine MRPS2 and human MRPS2 is 77.13%. By comparison, the homology between murine and human cytosolic ribosomal protein subunit 10 is 97% (Genecards).

2.0 MATERIALS AND METHODS

To complete this experiment, we used the chemicals, kits, antibodies and machines listed in tables 1, 2, and 3 below. AM9780

2.1 MATERIALS

Table 1. Chemicals and Kits

Product	Manufacturer	Catalog #
4X Laemmli Sample Buffer	Bio-Rad	#161-0747
Antibiotic Antimycotic Solution (100x), Stabilized	Sigma-Aldrich	A5995-100ML
Bio-rad protein assay dye reagent concentrate	Bio-Rad	5000006
Bovine Serum Albumin	Sigma	A2153-50G
Bromochloropropane	Molecular Research Center	BP151
Cell Lytic™M Cell Lysis Reagent	Sigma	C2978-250ML
Cytoseal™ 60	Richard-Allan Scientific	8310-16
Dimethyl Sulfoxide (DMSO)	Fisher Biotech	BP231-1
Dulbecco's Modified Eagle Medium [high glucose]	Gibco	12100-046 10x1L
4',6-diamidino-2-phenylindole (DAPI)	Sigma-Aldrich	D9542-1MG
Disposable Cell Scraper	Fisher Scientific	08-100-241
Ethyl Alcohol, 200 Proof	Decon Laboratories, Inc.	04-355-222
Fetal Bovine Serum	Sigma-Aldrich	12303C-500ML
Glycine	Fisher Bioreagents	BP381-5
Geneticin	Gibco	10131-027
Halt™ Protease Inhibitor Cocktail, EDTA-free (100X)	Thermo Scientific	78437
HEPES	Fisher Bioreagents	BP310-500
Isopropanol		
LB Agar, Miller	Fisher Bioreagents	BP1425-500

Table 1 Continued		
LB Broth, Miller	Fisher Bioreagents	BP1426-500
2-Mercaptoethanol	Bio-Rad	#161-0710
Methanol	Fisher Chemical	A454-4
Mini-PROTEAN® TGX™ Gels, 10-well comb, 50µl	Bio-Rad	456-9034
Nuclease-Free Water	Ambion	AM9932
Odyssey® Blocking Buffer (PBS)	Li-Cor	927-40000
One Shot® TOP10 Chemically Competent E. coli	Invitrogen	C404006
Phosphate Buffered Saline	Lonza	17-516F
Protease Inhibitor Cocktail	Sigma-Aldrich	P1860-1ML
Puromycin 10 mg/ml	Gibco	A11138-02
Sodium Bicarbonate	Fisher Scientific	SS33-3
RNAse Zap®	Ambion	AM9780
TOPO TA Cloning® Kit Dual Promoter pCR® II-TOPO® Vector	Invitrogen	K4600-01
Tris Base	Fisher Bioreagents	BP152-5
Triton®-X-100, electrophoresis grade	Fisher Biotech	BP151-500
TRIzol™ Reagent	Invitrogen	15596018
Trypsin-EDTA Solution	Sigma	T4049-100ML
TWEEN 20	Fisher Bioreagents	BP337-500

Table 2. Antibodies

Antibody	Company	Catalog #
Alexa fluor 488 donkey Anti-Rabbit IgG	Invitrogen	A21206
Alexa fluor 594 donkey Anti-mouse IgG 1/1000	Invitrogen	A21424
c-myc (A-14)-G antibody produced in Goat	Santa Cruz	sc-789-G
IRDye 680LT conjugated donkey anti-goat IgG	Licor	926-68024
IRDye 800 goat anti-mouse IgG1	Licor	926-3250
Anti-MRPS2, antibody produced in mouse, purified immunoglobulin	Sigma-Aldrich	SAB1407444-50UG
Mouse Anti-fibrillin Monoclonal Antibody raised against human fibrillin 1	Chemicon	MAB1919
Rat Lung α-Elastin Goat polyclonal antiserum	Elastin Products Company, Inc.	RA75

Table 3. Machines

Machine	Manufacturer	Catalog #
Cimarec®2 Hotplate	Thermolyne	HP88857104
Cellometer® Mini	Nexcelom	1001201
Centrifuge 5424R	Eppendorf	022620461
Centrifuge 5702	Eppendorf	5702000019
Digital Dry Bath	Labnet International Inc.	D1200
Electrophoresis Power Supply EPS 30	Amersham Pharmica Biotech	18-1130-01
Excella E24 Incubator/Shaker	New Brunswick Scientific	14-285-732
GeneAmp® PCR System 9700	Applied Biosystem	N8050200
Isotemp 228 Water Bath	Fisher Scientific	15-462-28Q
NanoDrop 2000c Specrophotometer	Thermo Scientific	ND-2000C
NUAI Laminar Flow Hood		
Olympus CKX41 Centrifuge	Olympus Life Science	
PB5001 Scale	Mettler Toledo	PB5001-S/A,PB5001-S/M
Power PAC 3000	Bio-Rad	51907-1
Sorvall Legend XIE Centrifuge	Thermo Scientific	75004505
Steri-Cycle CO_2 Incubator, HEPA Class 18	Thermo Electron Corporation	201370
Synergy UV	Millipore Corporation	CDUFB1001
UltraBasic UB-10 pH meter	Denver Instrument	
VariMix Platform	Thermoline	M79735
Vortex Genie	Scientific Industries Inc.	12-812

2.2 METHODS

2.2.1 Production and verification of mutant cells

2.2.1.1 Design of guides and insertion into plasmid vector

Three sets of CRISPR-associated guides were designed to target exons 2, 3, and 4 of the rat MRPS2 gene. These exons were selected for targeting because they form the bulk of the MRPS2 transcript and include highly-conserved regions that are likely of biological significance. Using a tool designed by Dr. Zhang of MIT, (Ran et al., 2013)we designed the 3 sets of guides to maximize the possibility of obtaining mutants. The PX495 plasmid contains constitutively expressed genes for both ampicillin and puromycin resistance, which allows for selection against bacteria and eukaryotic cells lacking the plasmid respectively. The expression of the guide RNA is driven by a U6 promoter, and the plasmid encodes a Cas9 nuclease containing a nuclear localization signal (Figure 1). The expression of Cas9 is driven by a cytomegalovirus hybrid enhancer/promoter. Guide RNA sequences were designed as pairs of complementary synthetic oligonucleotides modified at their 5'-ends with a phosphate group to facilitate ligation into the PX495 plasmid digested with the BbsI restriction endonuclease. After ligation, competent Top-10 *E. coli* cells were transformed with the recombinant plasmids were transformed, and were plated onto LB Agar plates containing 50µg/ml ampicillin and left to grow overnight in an incubator at 37°C. The following day, 12 *E. coli* colonies per construct were picked and placed in tubes containing 10mL LB medium with 50µg/ml ampicillin, and left in a shaking incubator to grow overnight at 37°C. The following day, plasmid DNA was isolated from these colonies

using a mini-prep kit (Qiagen). The extracted plasmid DNA was subjected to agarose gel electrophoris to identify the plasmid clones containing the insert. The band corresponding to the plasmid with the insert was cut out and purified with a gel purification kit (Qiagen). The insert region of the purified plasmid was examined using Sanger sequencing to confirm that the desired guides had been successfully cloned into the vector.

Table 4. Guide Sequences

Guide	Sequence	# offtarget sites (# offtarget sites in genes)	least #mismatches (#sites w/ least # of mismatches)
E2 Guide	5’ CCGCTCCGGCTGTGCTGACC 3’	113 (17)	2 (3)
E3 Guide	5’ GTCCCCGCAGTCAGCGAGCC 3’	291 (27)	3 (9)
E4 Guide	5’ TTCGAGGCCCGAGTACACCT 3’	39 (5)	3 (2)

Table 5. Px459 Sequencing Primer

Primer Name	Description	Sequence
LKO. 1 5’	Px459 CMV fw seq primer	5’ CGCAAATGGGCGGTAGGCGTG 3’

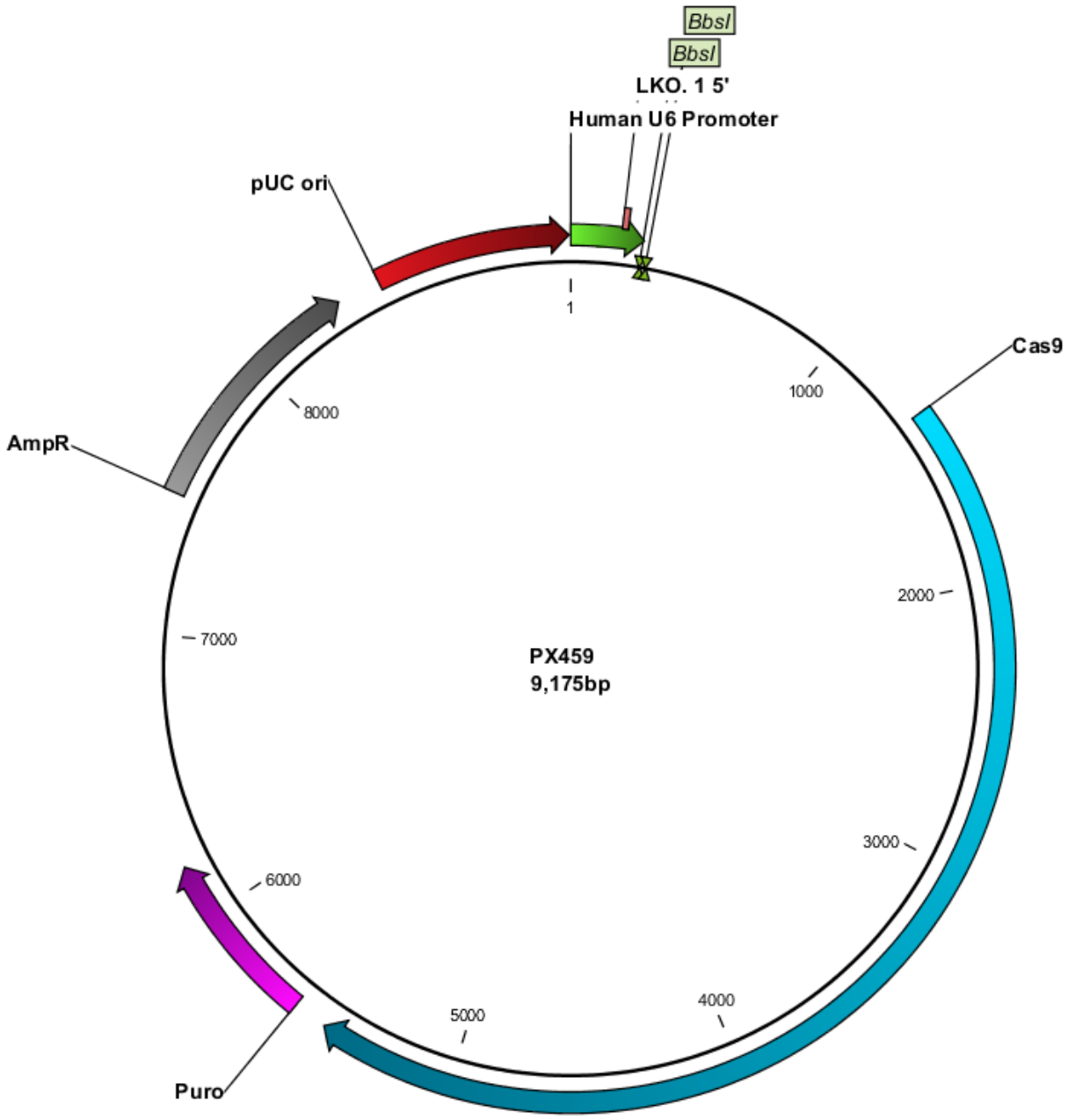

Figure 1. Px459 plasmid vector.
Legend, clockwise from top: U6 promoter, LKO 1.5 sequencing primer region, BbsI cloning sites, Cas 9 nuclease sequence, Puromycin resistance cassette, Ampicillin resistance cassette, pUC origin of replication

2.2.1.2 Transfection, selection, and expansion of RFL6 cells

A vial of frozen RLF6 cells was thawed and seeded into a 10-cm dish (Falcon) and transferred to 2 6-well plates. When the cells reached 80% confluence, plasmids were transfected

into 10 of the 12 wells. 3 wells per exon were transfected with plasmids containing the guides corresponding to each exon, and an additional well was transfected with an unmodified version of the plasmid as a negative control. The 2 remaining wells were used as controls; one well was treated with transfection reagents but no plasmid, and the other well was not treated with any transfection reagents, nor was any DNA introduced. The cells were exposed to the lipofectamine-plasmid complex for 24 hours, at which point the media was aspirated and replaced with Dulbeco's modified Eagle medium (DMEM) containing 10% fetal bovine serum (FBS) and 1% antibiotic-antimycotic solution (ABAM). After 24 hours, the regular 10% FBS 1% ABAM DMEM was replaced with 10%FBS 1%ABAM DMEM containing 1.5 µg/mL puromycin to select for cells transfected with the plasmid. At 1 week, the cells were expanded from the wells into 10-cm dishes (Falcon). After 2 weeks, the 2 dishes containing un-transfected cells contained no live cells. Due to low survival of cells after employing this selection timetable, a second round of selection with modified parameters was employed: all the conditions described above were identical, except the selection period was shortened to one week and the concentration of puromycin in the media was decreased to 1µg/ml. In both cases, surviving cells were expanded into progressively larger plates. When these became confluent, the cells were expanded into 2 15-cm plates per transfection; one 15-cm plate per transfection was frozen in 10%DMSO for later use while the other was harvested for DNA using a DNeasy Blood & Tissue Kit (QIAGEN).

2.2.1.3 Clonal isolation of RFL6 mutants

After confirming mutations in the RFL 6 transfectants, we proceeded to isolate clonal populations of RLF6 cells using a technique of serial limiting dilutions using 96-well plates (Corning.) Colonies of cells representing the daughters of single cells were identified by

microscopy and grown to confluence, at which point they were trypsinized and expanded to 24-well plates (Corning.) Individual clones were grown and expanded as they reached confluence into 3.5-cm dishes, 5-cm dishes, and 10 cm dishes. Clones were then harvested for DNA extraction. Selected clones were seeded onto coverslips and subjected to immunohistostaining to visualize elastin and tropoelastin expression in mutants compared to wild-type RLF6 cells.

2.2.1.4 Analysis of RFL6 cell DNA

The DNA obtained from the 15-cm plates was amplified using PCR primers corresponding to each targeted exon. The amplified exonic DNA was inserted into TOP 10 competent E. coli and plated onto ampicillin-containing LB Agar plates. Clones were picked and amplified in LB media containing ampicillin in a shaking incubator, and the DNA isolated using a Maxi Prep kit (QIAGEN). 6 clones per exon were sent for sequencing of the corresponding targeted regions.

2.2.1.5 Design of Myc-tagged MRPS2 construct

To verify the affinity of the MRPS2 antibody for MRPS2, two c-myc fusion genes were produced using the Gibson Assembly® Cloning Kit (New England BioLabs). Two sets of PCR primers, one of which flanks the entire MRPS2 transcript and one of which spans from the start codon to a premature stop in Exon 2, were used to amplify DNA from the human MRPS2 gene, which was then inserted into the pcDNA3.1(+)/myc-His B plasmid (Figure 2). The plasmid was transformed into using NEB® 5-alpha competent *E. coli*, clones were isolated and plasmid DNA extracted using a MaxiPrep kit (Qiagen). The insertion of the cDNA sequences into the plasmid was confirmed using Sanger sequencing. (fig) One clone each for wild type and truncated MRPS2 transfected into RFL6 cells using Lipofectamine 3000 transfection reagent

(ThermoFisher). Transfected cells were subjected to selection with 200 μg/mL geneticin to obtain stably transfected cell lines.

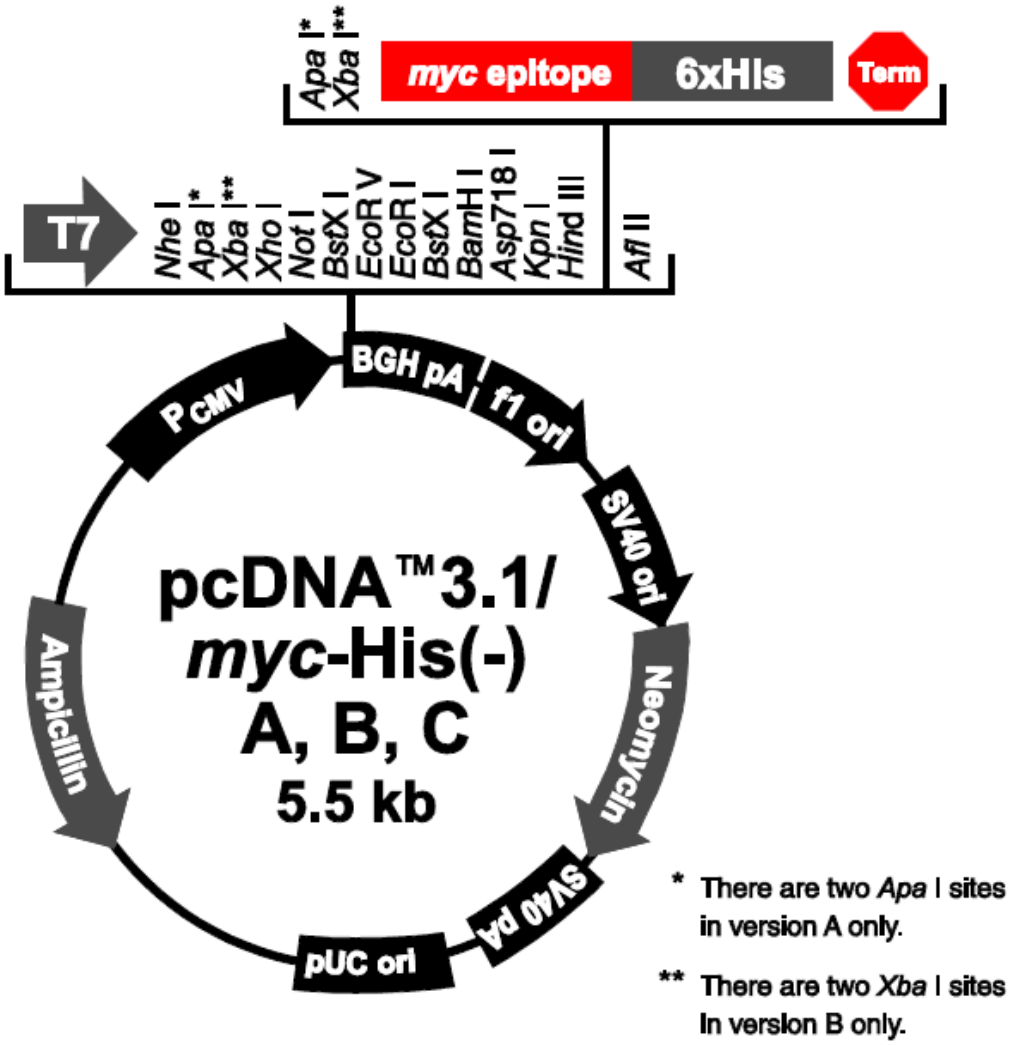

Figure 2. The map of the pcDNA *myc-His(-)B* 3.1 plasmid vector.
Legend, clockwise from top: T7 promoter, restriction sites, *myc* polypeptide sequence, polyhistidine-tag, termination signal, f1 origin of replication, SV40 origin of replication, Neomycin resistance cassette, SV40 poly-A, pUC origin of replication, Ampicillin resistance cassette, CMV promoter

2.2.2 RNA Analysis

2.2.2.1 RNA Isolation

RNA from wildtype, E4 mutant, and E3 mutant cell lines, as well as a cell line that was transfected with the PX459 plasmid and cloned but not found to contain any mutations, was obtained using the TRIzol® extraction method for RNA isolation. One 15-cm dish per cell line was treated with 8mL Trizol® and RNA was isolated using a method similar to that described in (Rio et al., 2010) except with 1-bromo-3-chloropropane (BCP) (Chomzynski 1995). The media from one 15-cm plate per cell line was aspirated, and replaced with 8mL Trizol. After 5 minutes of incubation, the trizol/nucleoprotein complex was mixed vigorously with 1 mL of BCP per sample, then incubated for 3 minutes. The tubes were centrifuged at 12,000 g for 12 minutes at 4°C to separate the protein and DNA phase from the RNA phase. The supernatant containing the RNA was transferred to tubes containing 4mL of ice-cold isopropanol per sample, shaken vigorously for 24 seconds, and left sitting for 12 minutes before being transferred back to the centrifuge and spun again at 12,000g for 12 minutes at 4°C. The supernatant was carefully decanted, and the RNA pellet was washed with 70% Ethanol in ddH_2O, then centrifuged for 6 minutes at 4°C. The ethanol was carefully poured out, and the pellet allowed to air-dry for 12 minutes. The dried RNA pellets were each dissolved in 160μL of nuclease-free water. These stock solutions were measured using the Nanodrop 2000 (Thermo Scientific), and used to create standardized 100ng/μL solutions of RNA.

2.2.2.2 Reverse Transcription

To get an accurate measurement of MRPS2 mRNA levels in the different cell lines 700 nanograms of RNA was used to create cDNA copies by reverse transcription (Superscript® IV

First-Strand cDNA Synthesis Kit from Thermo Fisher). The cDNA was then used to quantify MRPS2 mRNA levels using TaqMan® qPCR probes for rat MRPS2 and human GAPDH (rat GAPDH can be detected using human GAPDH probes, due to high sequence homology). cDNA was pipetted into 16 wells per sample, (8 replicates for GAPDH and 8 replicates for MRPS2) to a final dilution of 1/45, to minimize error.

Primers were designed to flank exons 3 and 4 to determine the relative abundance of the various truncated or expanded mRNA transcripts (see table and figure below.) The primers were designed such that the PCR products would be small enough for expansions and deletions to be readily detectable on a gel.

Table 6. Primers for amplification of cDNA copies of mRNA

Location	Sequence
Exon 1	5’ CTCACACGCATGGCCAAA 3’
Exon 2	5’ CATCTCAGTCCACGCGCCTA 3’
Exon 4	5’ GCAACCGGCTTTATGTCCCA 3’
Exon 5	5’ GGCGGTTCCCAAAGATGTAT 3’

Figure 3. Relative positions of PCR primers on the *MRPS2* cDNA.
Arrows indicate extent of primer regions and primer direction. Arrow length and exon length are to scale.

Complementary DNA from WT, E4 mutant, and both biallelic E3 mutant cells was amplified using the following primer combinations: E1 and E4, E2 and E4, E2 and E5, E1 and E5. After it was found that any combination involving E1 failed to yield any PCR product, the E2/E4 and E2/E5 amplifications were repeated and a gel image was captured. Based on the image, it was decided that the E2/E5 PCR products for the E4 mutant cDNA and both biallelic E3 mutant cDNAs would be good candidates for sequencing. The PCR products were cloned

into competent E. coli using the TOPO-TA Cloning Kit from Invitrogen and 14 clones per PCR product were expanded and the DNA was extracted using Monarch Mini-Prep kits and sent for sequencing.

2.2.2.3 Statistical Analysis

qPCR data is presented as mean ± SD. All statistical analyses were preformed using R statistical software, v. qPCR assays were performed in octuplicate, and the mean was used for statistical analysis. Statistical significance was set at $p < .05$.

2.2.3 Protein Analysis

2.2.3.1 Protein extraction

Secreted proteins were collected by washing 15cm plates of confluent cells with warm PBS 3 times, then incubating the plates with 15ml of serum-free DMEM per plate overnight. The media was then centrifuged for 12 minutes at 4000rpm at 4°C to remove debris and dead cells, and the supernatant was transferred to a concentrating filter with 3 kilodalton pores (Amicon). The media was centrifuged at 4000rpm at 4°C to concentrate it to a final volume of <500µL.

Cellular proteins were collected by lysis and homogenization. Confluent 15cm plates were washed 3 times with cold PBS, then treated with 1175µL Cell Lytic M lysis buffer supplemented with 10 µl protease inhibitor and 10 µl phosphatase inhibitor. The cells were put on a shaker with light shaking for 5 minutes at 4°C, and scraped with a cold cell scraper. The resulting lysate was transferred to a cooled glass homogenizer and liquefied with 24 strokes. Then, the lysate was transferred to a 1.5ml reaction tube and centrifuged at 13000 rpm at 4°C for 20 minutes.

2.2.3.2 Protein concentration verification

Both secreted proteins and cellular proteins were quantified using standard curves. Bovine serum albumin was diluted to final concentrations of 2µg/mL, 4µg/mL, 6µg/mL, 8µg/mL, and 10µg/mL, and mixed with either lysis buffer or serum-free DMEM to a final concentration of 1µl/mL, an mixed with water and 200µL Bradford's reagent to a final volume of 1ml. The protein samples were mixed with water and 200µL Bradford's reagent to a final concentration of 1µL/mL and a final volume of 1mL. The samples were incubated in the dark at room temperature for 30 minutes and the absorbances were measured with a Nanodrop 2000 spectrophotometer (Thermo Scientific.) The resulting curves were used to determine concentrations of the protein samples.

2.2.3.3 SDS-PAGE Electrophoresis

Mercaptoethanol and 4x Laemmli Buffer were mixed in a 1:9 ratio, to create a denaturing loading buffer, which was then mixed with the protein samples and incubated at 95°C on a heating block for 5 minutes. The samples were then pipetted into wells of a 4-20% Mini-Protean TGX precast gel (Biorad), with total protein standardized to 60µg per well for the lysate protein samples, and 80µg per well for the secreted protein samples. The gel was placed in a cell filled with ice-cold running buffer (9g tris base, 43.2g glycine, 1200mL water, 15mL 10% SDS) and connected to a power-pack. The cell was placed in an ice bucket and the gel was subjected to constant voltage of 100V for 75 minutes.

2.2.3.4 Membrane transfer

After 75 minutes, the gel was removed from the housing and carefully transferred to blotting buffer (2.4g Tris, 11.5g Glycine, 800ml H_2O, 200ml Methanol) where it was allowed to equilibrate for 15 minutes. Towards the end of this incubation, a piece of polyvinylidene fluoride (PVDF) membrane for each gel was activated in methanol for 15 seconds then allowed to equilibrate in blotting buffer for 5 minutes. A transfer assembly was then constructed in the following order: Cathode, sponge, 4 pieces of filter paper, gel, PVDF membrane, 4 pieces of filter paper, sponge, and anode. The assembly was submerged in ice-cold blotting buffer along with an ice pack and subjected to a constant voltage of 100V for one hour.

2.2.3.5 Immunodetection

After membrane transfer, the PVDF membrane was washed in PBS, rinsed in water, then dried between two filter papers overnight at 4°C. The membrane was then immersed in 100% methanol for 1 minute, rinsed in ultrapure water, and wet in 1X PBS for 1 minute. The membrane was then incubated in PBS-based Odyssey Blocking Buffer (Licor) on a shaker with gentle shaking at room temperature for one hour. The membrane was cut, and the part containing the rightmost 3 lanes (ladder, c-myc-tagged full-length MRPS2, and c-myc-tagged truncated MRPS2) was immersed in a solution of Odyssey Blocking Buffer containing 1:500 diluted c-myc antibody raised in Goat and Tween-20 at a final concentration of .2%. The remainder of the membrane was immersed in a solution of Odyssey Blocking Buffer containing anti-MRPS2 antibody raised in mouse at a dilution of 1:500 and Tween-20 at a final concentration of .2%. The primary antibody incubation was performed overnight at 4°C on a shaker with gentle shaking. Following primary antibody incubation, the membrane was washed 4 times for 5 minutes each with 1x PBS with tween 20 at a final concentration of 0.1% (PBS-T) on a shaker

with vigorous shaking at room temperature. The membranes were then incubated in a solution of Odyssey Blocking buffer with Tween-20 at a final concentration of .2 and SDS at a final concentration of 0.01%, as well as secondary antibodies at a dilution of 1:20,000 (IRDy 800CW goat anti-mouse IgG1 from Licor for MRPS2, and IRDye 680LT conjugated donkey anti-goat IgG from Licor for c-Myc) for 1 hour at room temperature with gentle shaking. Following another wash step identical to that described above, the blot was rinsed in 1xPBS, then placed between two kimwipes to dry.

2.2.4 Immunostaining

Wildtype cells, cells from the E4 mutant cell line, and cells from both E3 mutant cell lines were seeded on glass coverslips at a concentration of $1x10^5/cm^2$ and allowed to grow for 5 days. The cells were washed 3 times with cold PBS, fixed in 4% paraformaldehyde in PBS with gentle shaking at 4°C for 20 minutes, then washed 3 times with .3M glycine in PBS for 15 minutes each time on a shaker at room temperature. The cells were then blocked for an hour at room temperature in a solution of PBS with .3M glycine, 1% donkey serum, and 3% bovine serum albumin. Following another 5 15-minute PBS washing steps at room temperature, the cells were treated with a solution of 3% bovine serum albumin in PBS supplemented with tropoelastin antibody diluted 1:100 and fibrillin antibody diluted1:400. Following another 5 15 minute PBS washing steps at room temperature, the cells were treated with a solution of solution of PBS with .3M glycine, 1% donkey serum, and 3% bovine serum albumin supplemented with secondary fluorescent antibodies and incubated in the dark at room temperature for 1 hour. Following another 3 15 minutes PBS washing steps at room temperature, the cells were incubated in a solution of PBS with 4',6-diamidino-2-phenylindole (DAPI) in a 1:1000 dilution

on a shaker in the dark at room temperature for 20 minutes. The coverslips were then subjected to a final washing stage, with 5 5-minute washes with PBS supplemented with .1% Triton-X-100. The coverslips were then rinsed with water, carefully removed from the plates with a spatula, and left to dry cell-side-up for 30 minutes in the dark. 10 µl of Cytoseal™ 60 was dropped onto the center of glass microscope slides and the coverslips were then pressed cell-side-down onto the slides, which were then left to dry in the dark.

3.0 RESULTS

3.1 IDENTIFICATION AND CHARACTERIZATION OF MUTANT CELL LINES

Sanger sequencing of PCR products of 42 cloned cell lines revealed three cell lines with apparent mutations in the targeted regions of *Mrps2*. To better resolve the mutations in these cell lines, PCR amplified target regions were subjected to plasmid cloning. Sanger sequencing of plasmid clones of the three mutant cell lines identified one cell line with a deletion mutation in a single allele of *Mrps2*, in exon 4, and two cell lines, each with unique deletion and insertion mutations in both alleles of exon 3. The WT/mutant heterozygote cell line -designated simply 'E4'- contained a 34bp deletion on one copy of the *Mrps2* gene, while the other copy of the *Mrps2* contained no detectable changes from wildtype. One mutant/mutant compound heterozygote cell line -designated '11'- contained a 51 bp insertion and 1bp deletion in exon 3 of one copy of the *Mrps2* gene and a 154-bp deletion in exon 3 of the other copy. [(c.123_124ins51 ; c.180delC (p. P60Pfs*16), g.2060_2105del (p.D34Ffs*70)]. The other mutant/mutant compound heterozygote –designated ‘10’- contains a 66bp deletion in exon 3 of one copy of the MRPS2 gene and a 39bp insertion in exon 3 of the other copy (g.2039_2213del; c.123_124ins39).

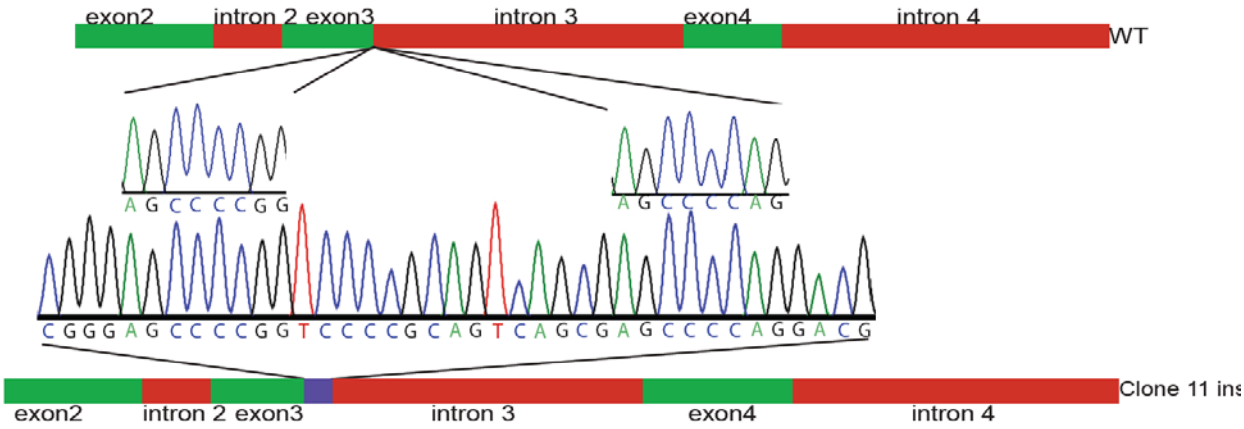

Figure 4. A schematic representation of the insertion mutation in clone 11.
DNA from clonal cell lines and wildtype cells was extracted and the target region amplified using PCR. PCR products were cloned into *E. coli* to examine individual alleles of *Mrps2* via Sanger sequencing. Exons (green), introns (red), and inserted region(blue) are drawn to scale. Sequence traces from selected regions of wildtype (WT) and biallelic clone 11 mutant cells (Clone 11 ins) have been aligned to highlight homology and differences.

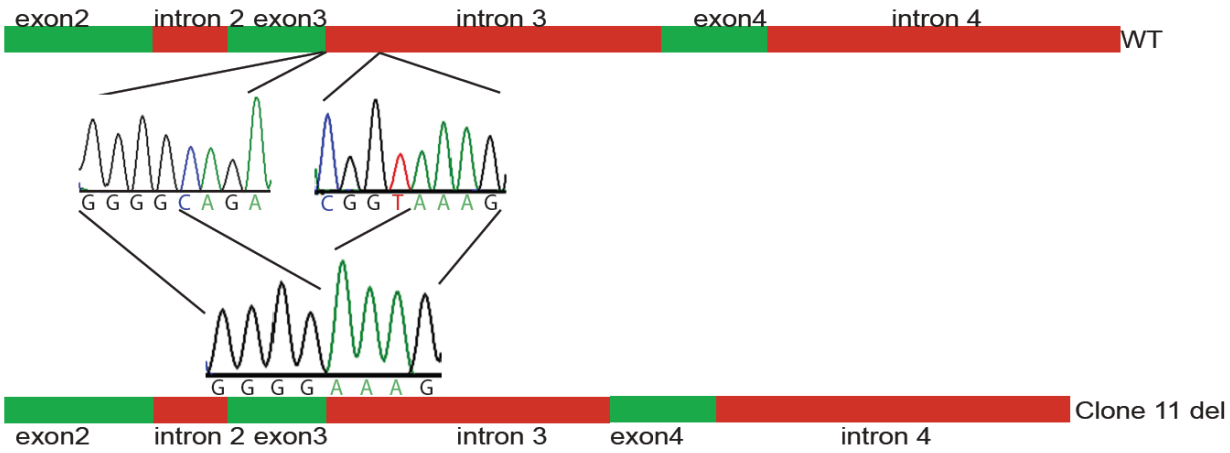

Figure 5. schematic representation of the deletion mutation in clone 11.
DNA from clonal cell lines and wildtype cells was extracted and the target region amplified using PCR. PCR Products were cloned into *E. coli* to examine individual alleles of *Mrps2* via Sanger sequencing. Exons (green) and introns (red) are drawn to scale. Sequence traces from selected regions of wildtype (WT) and biallelic clone 11 mutant cells (Clone 11 del) have been aligned to highlight homology and differences.

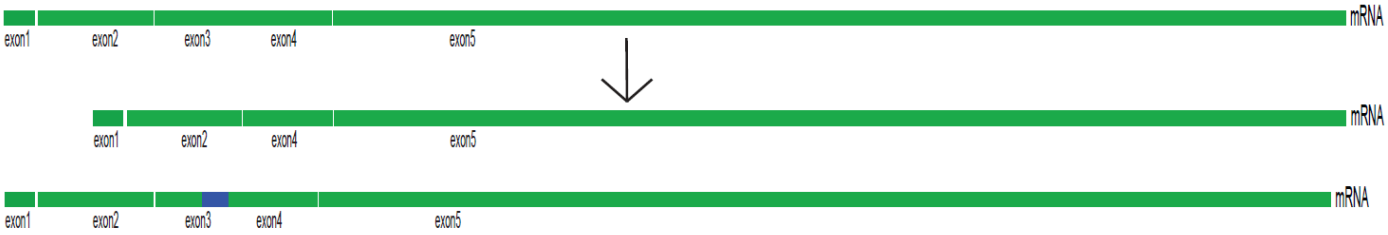

Figure 6. A schematic representation of two types of mRNA variants observed in clones 10 and 11.
From top: Wildtype mRNA size, Exon 3 skip mRNA product, insertion/deletion mRNA product.

The predicted consequences of the mutations are varied. In the case of E4, the deletion results in a premature termination at the 17th amino acid position of exon 5 (under normal conditions, *MRPS2* is predicted to terminate at amino acid position 195 of Exon 5, which is where the first stop codon is in the wildtype reading frame). However, it is unknown whether the bulk of exon 5 actually serves a biological function or whether it is proteolytically removed during processing.

In cell line 10, the 66bp deletion in exon 3 results in the deletion of the last 64 bases of exon 3, causing a frameshift that leads to the predicted premature termination of translation at amino acid position 7 of exon 4. The 39bp insertion on the other allele of exon 3 is not predicted to result in a premature termination of protein synthesis.

In the case of mutant cell line 11, the combination of the 51bp insertion and the single base deletion results in a frameshift that results in a premature termination at the 16 amino acids residues downstream of the deletion, in the 16th amino acid of exon 4. On the other allele, the 154-bp deletion results in the deletion of the last 44 bases of exon 3, resulting in a frameshift that results in a premature stop 70 amino acids downstream of the deletion.

3.1.1 Consequences of *Mrps2* mutations at the mRNA level

Raw Ct (threshold cycle) values were converted to expression-fold change values using a classic $2^{-\Delta\Delta CT}$ method with pairwise comparisons (see supplemental calculations) (Schmittgen and Livak, 2008). The analysis identified no statistically significant reduction in *Mrps2* mRNA levels for either the E4 cell line or a cell line that was subjected to the same treatment as the mutant cells but found to contain no mutations. There was, however, a 39.3% reduction in *Mrps2* levels for exon 3 mutant 10 (SD: 3.66%), and a 43.1% reduction in *Mrps2* levels for Exon3 mutant 11 (SD: 13.78%) (see graph 1).

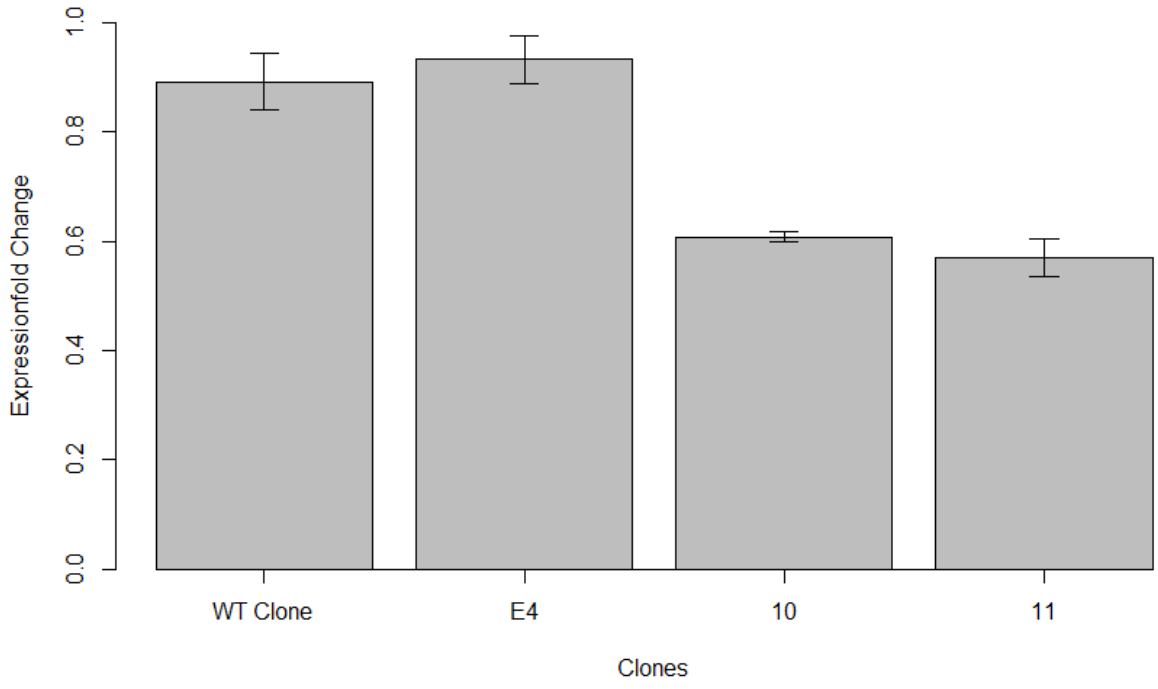

Figure 7. Expressionfold changes in MRPS2 mRNA
Significance bars represent 95% confidence intervals.

Table 7. *Mrps2* cDNA clone sequencing results

E3 Clone 10	
c.43_160del [total skipping of Exon 3]	11
c.43_160delins87	2
c.129_130instGCGCGCTCGCTCGCTCACTGAGGCCGGGCGACCAA	1
Total	14
E3 Clone 11	
c.116_160delinsCAGAACCCCTGTGGCCTG	7
c. 43_160del [total skipping of Exon 3]	1
Wildtype	1
Total	8

In analyzing sequence data for the two biallelic mutant clones (Table 6), we confirmed the existence of PCR products corresponding to mRNA transcripts with complete knockout of Exon 3 in both the Clone 10 and Clone 11 samples, as well as insertion and deletion products unique to Clone 10 and Clone 11. The clone 10 found to produce three types of *Mrps2* transcripts: 11 cDNA clones showed a complete skipping of exon 3, in 2 cDNA products exon 3 was replaced by an 87 bp fragment corresponding to the final 87 bases of intron 3, and 1 cDNA clone with the insertion of a 36 bp sequence in the guide region. After removing 4 unreadable sequences, the *Mrps2* transcript produced by Clone 11 were represented by a total of 8 cDNA clones: 1 with a complete skipping of exon 3, 1 corresponding to the wildtype sequence, and 7 with a deletion of the final 48 bases of exon 3 and insertion of 17 bases from intron 3, corresponding to the 17 bases directly 3’ of the Clone 11 deletion.

The reasons the exon skip products are more abundant in the clone 10 population, while the insertion/deletion products are more abundant in the clone 11 population, likely involve the sequences of the insertions and the extent of deletions, and how they could affect recognition of splice sites by the spliceosome. In the case of clone 10, it could be that both the insertion and the deletion may induce exon skipping. Of note, the motif CAGattt appears at both the canonical

exon 3 – exon 4 splice junction and the new intron 3 - exon 4 splice junction. Using the Splice Site Prediction tool from the Berkely Drosophila Project, we verified that the new splice acceptor site is predicted to have comparable activity to the canonical intron 3 – exon 4 splice acceptor site (new acceptor site score: .98, canonical acceptor site score: .97)

In the case of clone 11, it seems that the mRNA product containing a partial deletion of exon 3 and insertion of part of intron 3 is the more abundant product, while transcripts with total skipping of exon 3 are comparably rare. It may also be possible that the reason mRNAs representing the insert mutation are not well-represented is that the transcripts are degraded via nonsense-mediated decay.

In the case of the insertion of 87 bases from intron 3 in the clone 10, the mutation is predicted to result in a premature stop 10 amino acid residues after the start of the insertion (p.Gly15Aspfs*11). The other insertions and deletions result in no predicted frameshift or premature termination.

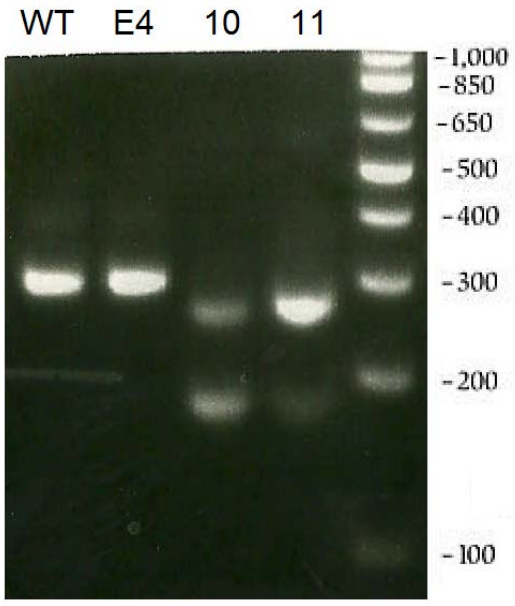

Figure 8. PCR amplification of cDNA.
Amplified region spans start codon through 465th base of coding region (121st base of Exon 4).

3.1.2 Western Blot

The Western blot obtained from the secreted protein fraction of cultured cells reveals a secreted protein around 8 kilodaltons in size that reacts with the anti-MRPS2 antibody. The cells transfected with the c-myc tagged MRPS2 display a band in the same size range when exposed to anti-c-myc antibody. There also appears to be a protein product around 90kD in mass that reacts with the c-myc antibody.

The intracellular protein sample containing protein extracts from the biallelic mutants did not yield a readable blot, but previous runs showed a protein band in the 15kDa range (Figure 9)

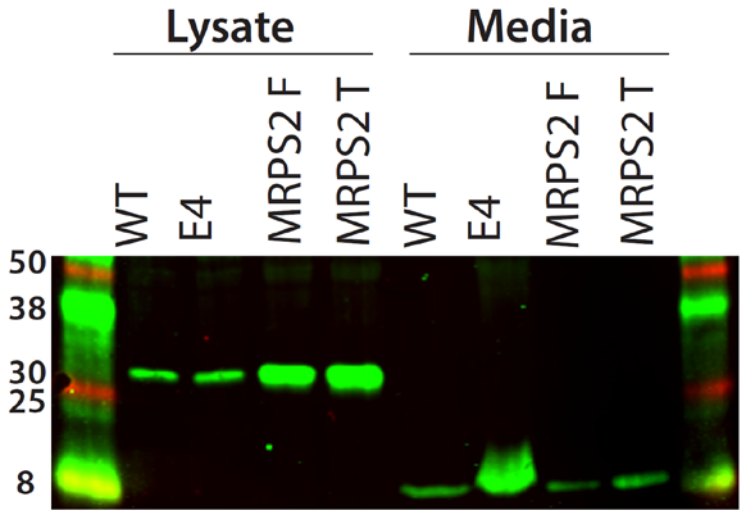

Figure 9. Immunoblotting for MRPS2 in mutant and overexpressing cell lines.
Lysate and concentrated conditioned media were collected from wildtype (WT), MRPS2 heterozygote mutant (E4), and cells stably transfected to express c-Myc-tagged full-length (MRPS2 F) or truncated (MRPS2 T) MRPS2. First and last lanes contain molecular weight standards. Numbers indicate molecular weight in kilodaltons.

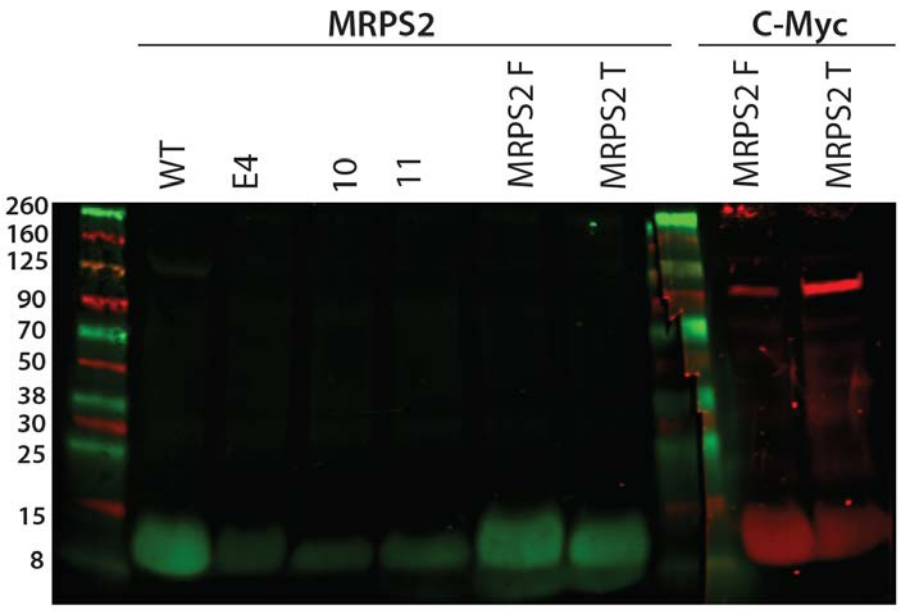

Figure 10. Immunoblotting for MRPS2 and c-Myc in mutant and overexpressing cell lines. Conditioned media was collected from wildtype (WT), MRPS2 heterozygote mutant (E4), biallelic mutant (10, 11), and cells stably transfected to express c-Myc-tagged full-length (MRPS2 F) or truncated (MRPS2 T) MRPS2. First lane and cut lane contain molecular weight standards. Lanes 2-7 were probed using an MRPS2 andtibody, whereas lanes 9 and 10 were probed for c-Myc. Numbers at the left side of the image indicate molecular weight in kilodaltons.

3.1.3 Immunostaining

Though the cells were all seeded at equal concentration, by the end of the 5-day waiting period, the cells on the WT and E4 coverslips were visibly more confluent than the cells on the cell line 10 and cell line 11 coverslips. There also appears to be a difference in tropoelastin morphology (Figure 11). The WT and E4 cell lines appear similar to each other in that the elastin is more fibrous, while in both biallelic mutant cell lines, the tropoelastin appears to be deposited in more evenly distributed sheets. Another notable difference is the presence of enlarged nuclei in cell line 10. Fibrillin morphology could not be analyzed because the primary antibody appears to have failed to demonstrate ECM specificity.

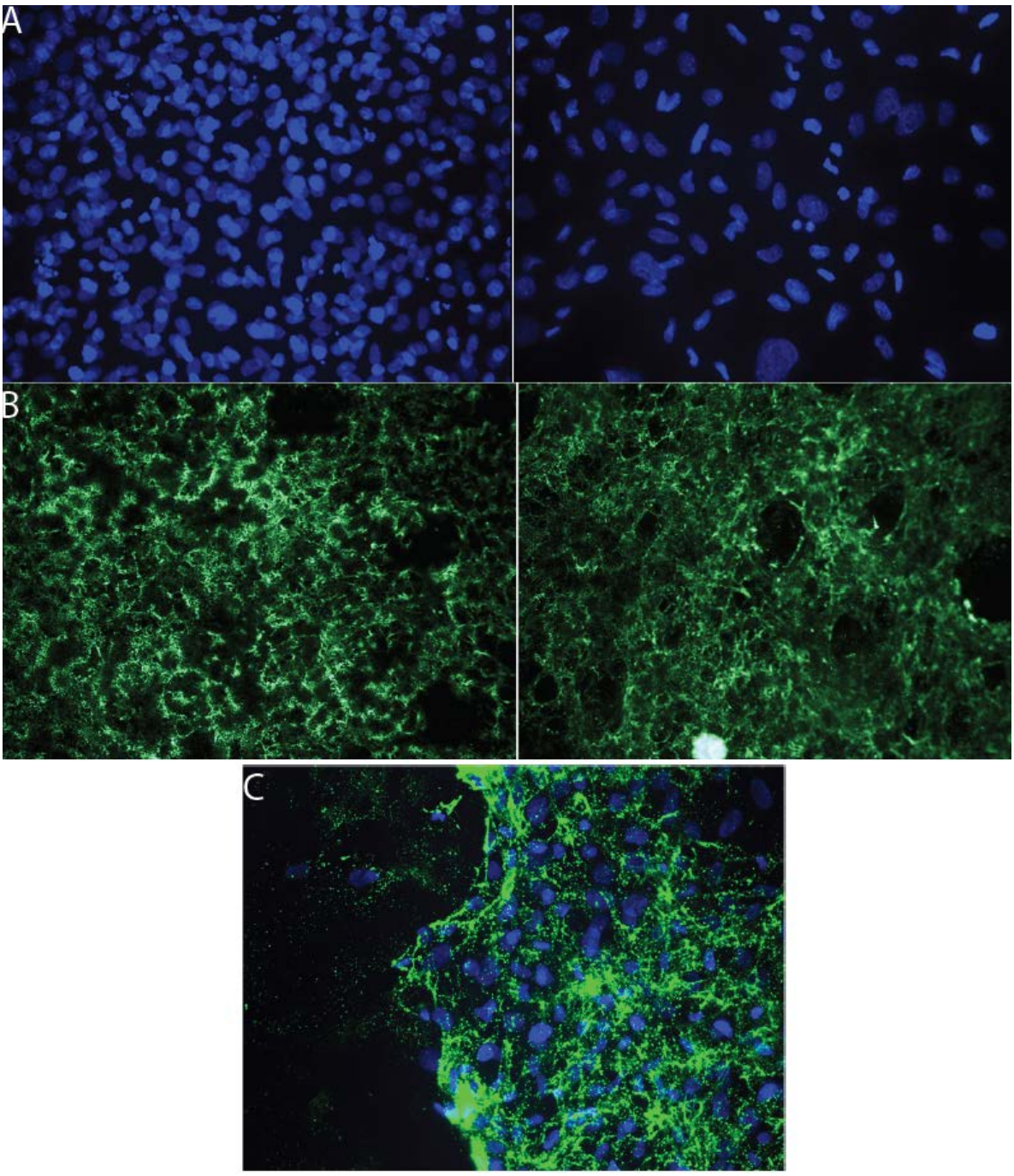

Figure 11. Fluorescent staining of biallelic mutant and wildtype cells.
Cells were seeded at a density of 300,000 cells/well and allowed to grow for 5 days before being fixed in paraformaldehyde and treated with tropoelastin antibody (green), and DAPI (blue). (A) Comparison of Wildtype (WT) and biallelic mutant 10 (10) nuclei. (B) Comparison of Wildtype (WT) and biallelic mutant 11 (11) tropoelastin. (C) Example of peeling in biallelic mutant 10, DAPI and tropoelastin overlay.

4.0 DISCUSSION

The experiment was successful in generating biallelic mutations in *Mrps2*, though the small quantity of mutants relative to the size of the clonal population leaves considerable room for improvement. The drawn-out process we had to employ to tailor the protocol to the difficult-to-transfect RFL6 cells –which was only briefly touched upon in this document - has reaffirmed the common wisdom that getting optimal results often requires considerable deviation from the protocols supplied by journals and manufacturers.

The proportions of cDNA sequencing products with either partial or complete deletions of exon 3 correspond to the relative intensity of bands observed when the PCR products are run on a gel. The difference in sizes of the bands also correspond with the difference between the sizes of the complete and partial deletions of exon 3.

The fact that a deletion that encompasses the exon-intron junction results in complete exon skipping is unsurprising, as the sequences of the exon-intron junctions are important for proper splicing of exons. Similar cases have been consistently documented in the literature. The fact that the exon skipping occurred predominantly in mutant 10 and was only observed in one clone isolated from mutant 11 is consistent with the fact that the deletion in clone 11 just barely reaches into intron 3, deleting only two nucleotides in the 5’ end of the intron, while the deletion in clone 10 deletes the first 110 base pairs in the 5’ end of intron 3.

What is surprising is that only sequences deletion of parts of exon 3 were detected in the PCR products obtained from amplifying cDNAs from mRNAs obtained from the two biallelic mutant cell lines. One might have expected to find sequences larger than wildtype transcripts corresponding to the insertions found in either cell line, but these do not appear to be represented in the sequences obtained from the clones.

The fact that tropoelastin deposition appears to be affected in the cell lines with biallelic mutations of *Mrps*2 is consistent with what was observed in the families of the two patients, but the data collected so far does little to elucidate precisely what the mechanism may be. The fact that the DAPI stain seems to show that the biallelic mutant cells possess enlarged nuclei is also useful. Swelling of the nuclei has been found to be associated with mitochondrial disease in mouse models, and there is evidence that this phenotype is correlated with oxidative stress (Wallace and Fan, 2009). Oxidative stress has been observed to result from disruption of electron transport chain function, so disruption of the formation of the mitoribosome, which is responsible for ETC assembly, leading to oxidative stress, is a likely culprit in the development of the phenotype observed in the patients (Jones, 2006).

While this explanation partially satisfies the question of how a direct link between molecular genetics could lead to the observed cellular phenotype, it fails to fully explain why fibroblasts and elastic fiber assembly in particular are affected, as wrinkly skin is not a universal manifestation. Given that the mitoribosome has evolved to specialize in the synthesis of ETC proteins, it is possible that disruption of different specific elements of the ribosome could lead to disruption of different specific ETC elements, leading to different phenotypes, but beyond that, not much more can be concluded from the results of this experiment and the available literature, and further analysis is needed. Perhaps the relationship is more simple, and the key is simply the

balance between the degree to which ROS species upregulation and ATP downregulation are affected. The accumulation of reactive oxygen species has been connected to the disturbance of the activity metalloproteases responsible for degrading fibrillin, which offers another possible mechanism for the manifestation of a wrinkly skin phenotype (Klein and Bischoff, 2011).

The Western blot is potentially very informative. The fact that the c-myc antibody reacted with the same protein product that reacted with the *Mrps2* antibody in the cells transfected with the c-myc-tagged *Mrps2* transcript indicates that the protein that the *Mrps*2 antibody is reacting with in the other samples is indeed a fragment of *Mrps2*. As the c-myc tag was affixed to the C-terminus of the *Mrps2*, we can infer that the fragments are C-terminal fragments of *Mrps2* that are proteolytically cleaved during processing. The lowered intensity of the *Mrps2* signal in the mutant cell lines compared to the wildtype cell line is consistent with the lowered mRNA abundance due to nonsense-mediated decay and/or failure of the antibody to bind as effectively to *Mrps2* due to altered amino acid sequence caused by frameshifts and deletions of large portions of the protein. It should be noted that a the middle of a region that is highly conserved between the Rat and Human versions of the protein lies roughly 70 amino acid residues (~8 kilodaltons), upstream of the C terminus. The fact that the fragment is found in the extracellular space may be related to the fact that the extracellular matrix morphology is altered, but determining a mechanism for such an effect

5.0 CONCLUSIONS

Taken together, these data present a tantalizing picture of MRPS2's function in the cell. Further investigation is needed to determine the significance of our findings. Of highest priority is the analysis of indicators of mitochondrial function and characterization of ECM dysfunction.

The observation that growth seems to be impaired in the biallelic mutant cells merits some follow-up. During the preparation of slides, the mutant 10 and 11 cells were more susceptible to sloughing off from the coverslips than the WT or E4 cells, despite being less confluent. All else being equal, sloughing will occur more readily in overconfluent cells rather than underconfluent cells, so this paradoxical observation suggests that the biallelic mutant cells are not merely growing slowly, but also failing to adhere properly for some reason. A cell adhesion assay will shed light on the severity of this dysfunction. One of the more pressing questions is precisely how the disruption of mitoribosomal formation could be causing disruption of the mutant cells. Untangling the complex network of cause and effect that could be at play here will require controlled study of several variables associated with fibroblast health. An ATP assay on cell lysate could determine whether mitochondrial energy production is being altered. Oxygen and pH flux experiments using a Seahorse instrument could be used to quantify oxidative phosphorylation and glycolysis; this could help clarify how the production of ATP is being disrupted, and whether disruption of ETC formation could be causing some sort of diversion of the normal cellular respiration pathway. Retrying the fibrillin stain and staining for

other ECM components such as fibronectin could provide further information on how ECM morphology is affected. In the long term, if the knockdown process were to be repeated to produce more mutants with more severe *Mrps2* mutations (perhaps generating another mutation in the existing mutants), it could be productive to use a more recent version of the Px459 plasmid, as the original version that was used in the experiment was later found to possess a less efficient version of the puromycin resistance gene. This flaw was rectified in the more recent version of the plasmid, pSpCas9 (BB)-2A-Puro (PX459) V2.0. Finally, a more thorough characterization of the secreted *Mrps2* fragment would be valuable, and this could be obtained by immunoprecipitation.

BIBLIOGRAPHY

Baldwin, A.K., Simpson, A., Steer, R., Cain, S.A., and Kielty, C.M. (2013). Elastic fibres in health and disease. Expert Rev Mol Med *15*, e8.

Berk, D.R., Bentley, D.D., Bayliss, S.J., Lind, A., and Urban, Z. (2012). Cutis laxa: a review. J Am Acad Dermatol *66*, 842 e841-817.

Bolar, N., Van Laer, L., and Loeys, B.L. (2012). Marfan syndrome: from gene to therapy. Curr Opin Pediatr *24*, 498-504.

Chuang, C.Y., Degendorfer, G., and Davies, M.J. (2014). Oxidation and modification of extracellular matrix and its role in disease. Free Radic Res *48*, 970-989.

Davis, M.R., and Summers, K.M. (2012). Structure and function of the mammalian fibrillin gene family: implications for human connective tissue diseases. Mol Genet Metab *107*, 635-647.

De Silva, D., Tu, Y.T., Amunts, A., Fontanesi, F., and Barrientos, A. (2015). Mitochondrial ribosome assembly in health and disease. Cell Cycle *14*, 2226-2250.

Freedman, B.R., Bade, N.D., Riggin, C.N., Zhang, S., Haines, P.G., Ong, K.L., and Janmey, P.A. (2015). The (dys)functional extracellular matrix. Biochim Biophys Acta *1853*, 3153-3164.

Gopisetty, G., and Thangarajan, R. (2016). Mammalian mitochondrial ribosomal small subunit (MRPS) genes: A putative role in human disease. Gene *589*, 27-35.

Hatakeyama, H., and Goto, Y. (2016). Concise Review: Heteroplasmic Mitochondrial DNA Mutations and Mitochondrial Diseases: Toward iPSC-Based Disease Modeling, Drug Discovery, and Regenerative Therapeutics. Stem Cells *34*, 801-808.

Jensen, S.A., Robertson, I.B., and Handford, P.A. (2012). Dissecting the fibrillin microfibril: structural insights into organization and function. Structure *20*, 215-225.

Jones, D.P. (2006). Disruption of mitochondrial redox circuitry in oxidative stress. Chemico-biological interactions *163*, 38-53.

Klein, T., and Bischoff, R. (2011). Physiology and pathophysiology of matrix metalloproteases. Amino acids *41*, 271-290.

Koc, E.C., Burkhart, W., Blackburn, K., Moyer, M.B., Schlatzer, D.M., Moseley, A., and Spremulli, L.L. (2001). The large subunit of the mammalian mitochondrial ribosome. Analysis of the complement of ribosomal proteins present. J Biol Chem *276*, 43958-43969.

Liang, C., Ahmad, K., and Sue, C.M. (2014). The broadening spectrum of mitochondrial disease: shifts in the diagnostic paradigm. Biochim Biophys Acta *1840*, 1360-1367.

Luciano, P., and Geli, V. (1996). The mitochondrial processing peptidase: function and specificity. Experientia *52*, 1077-1082.

Nouws, J., Goswami, A.V., Bestwick, M., McCann, B.J., Surovtseva, Y.V., and Shadel, G.S. (2016). Mitochondrial Ribosomal Protein L12 Is Required for POLRMT Stability and Exists as Two Forms Generated by Alternative Proteolysis during Import. J Biol Chem *291*, 989-997.

Oshima, T., Yamasaki, E., Ogishima, T., Kadowaki, K., Ito, A., and Kitada, S. (2005). Recognition and processing of a nuclear-encoded polyprotein precursor by mitochondrial processing peptidase. Biochem J *385*, 755-761.

Ran, F.A., Hsu, P.D., Wright, J., Agarwala, V., Scott, D.A., and Zhang, F. (2013). Genome engineering using the CRISPR-Cas9 system. Nature protocols *8*, 2281-2308.

Rio, D.C., Ares, M., Jr., Hannon, G.J., and Nilsen, T.W. (2010). Purification of RNA using TRIzol (TRI reagent). Cold Spring Harbor protocols *2010*, pdb prot5439.

Rosenbloom, J., Abrams, W.R., Indik, Z., Yeh, H., Ornstein-Goldstein, N., and Bashir, M.M. (1995). Structure of the elastin gene. Ciba Found Symp *192*, 59-74; discussion 74-80.

Sakai, L.Y., Keene, D.R., and Engvall, E. (1986). Fibrillin, a new 350-kD glycoprotein, is a component of extracellular microfibrils. J Cell Biol *103*, 2499-2509.

Schmittgen, T.D., and Livak, K.J. (2008). Analyzing real-time PCR data by the comparative C(T) method. Nature protocols *3*, 1101-1108.

Shokolenko, I.N., and Alexeyev, M.F. (2015). Mitochondrial DNA: A disposable genome? Biochim Biophys Acta *1852*, 1805-1809.

Urban, Z., and Davis, E.C. (2014). Cutis laxa: intersection of elastic fiber biogenesis, TGFbeta signaling, the secretory pathway and metabolism. Matrix Biol *33*, 16-22.

Wallace, D.C., and Fan, W. (2009). The pathophysiology of mitochondrial disease as modeled in the mouse. Genes & development *23*, 1714-1736.

Williams, C.C., Jan, C.H., and Weissman, J.S. (2014). Targeting and plasticity of mitochondrial proteins revealed by proximity-specific ribosome profiling. Science *346,* 748-751.